doi.org/10.1002/batt.202000001

3D Periodic Ion Transport Channel to Suppress Top Deposition toward Stable Lithium Metal Anode

Linhai Pan,[a] Jian Wang,[a] Zhifu Luo,[a, b] Zehua Zhao,[a] Yanyan Li,[a] Ishioma Egun,[a] and Haiyong He*[a]

3D structures have been widely used to suppress dendritic growth for stabilizing lithium metal anode. Unfortunately, it is hard to avoid lithium metal depositing on top of the framework, causing framework to lose its function. Here, we constructed a 3D periodic TiO_2 framework (3D-TiO_2) on copper foil using polystyrene beads as template. The poor conductivity of TiO_2 makes metallic lithium to nucleate on copper surface under framework. Combining with 3D periodic channels for fast ion transport, lithium metal gradually filled the whole space of framework. No lithium metal appeared on surface of 3D-TiO_2 electrode before filling up inner space. Meanwhile, large space provided by interconnected framework can ensure high loading of lithium, thereby suppressing the volume fluctuation during cycling. Additionally, batteries assembled by 3D-TiO_2 electrode exhibited excellent rate capability, owning to the fast ion transport supplied by 3D periodic structure. We believe that the combination of high capacity and frequency response in lithium metal anode could meet the challenge of the currently available devices.

1. Introduction

In recent years, high energy density batteries are needed due to the demand of electric vehicles, smart grid storage, and other electrical equipment. Therefore, rechargeable lithium metal batteries have inspired growing research interest in terms of high energy density.[1–2] Among various available candidates, lithium metal has been intensively pursued as a promising anode for lithium metal batteries given its low gravimetric density (0.53 g cm^{-3}), low potential (−3.04 V vs the standard hydrogen electrode), and high theoretical specific capacity (3860 mA h g^{-1}).[3–5] Unfortunately, the uneven plating/stripping of lithium and huge volume fluctuation induces lithium dendrite growth and low Coulombic efficiency, resulting in internal short circuit and safety hazard.[6–8]

Over past decades, considerable efforts have been devoted to improve the performance of lithium metal anodes. These strategies mainly included stabilizing solid electrolyte interphase (SEI) films with modification of electrolyte components,[9–11] constructing an artificial protective layer,[12–13] and using solid-state electrolyte.[14–16] These methods can partially mitigate the lithium dendrite growth, but cannot eradicate the growth of dendritic lithium. Once the lithium dendrites growth exceeded the endurance limit of the building protective layers, the cracking of SEI films would expose the fresh lithium metal to electrolyte and induce further side reactions (Figure 1a). Another promising approach was to accommodate lithium within a 3D framework to reduce the local current density, thereby suppressing dendrite formation.[17–20] Hence, various carbon nanostructures, metal and metal oxide scaffolds were prepared to regulate the lithium nucleation and depositing behavior. Wan et al. developed a lightweight nitrogen-doped graphitic carbon foams for uniform lithium nucleation/growth.[21] Braun et al. fabricated a sandwich composite anode consisting of gold nanoparticles pillared reduced graphene oxide to induce homogeneous lithium nucleation.[22] Although these scaffolds are effective in regulating the lithium nucleation and growth, precious metal nanoparticles or dopants are still required to lower nucleation energy of lithium metal. Additionally, various metal and metal oxide scaffolds with regular channels were also prepared to stabilize lithium metal anode. Zhu et al. stabilized the lithium metal anode through the space confinement and uniform curvature design of titanium dioxide nanotube arrays.[23] Guo et al. reported a copper current collector with vertically aligned microchannels for dendrite-free lithium deposition.[24] These metal and metal oxide scaffolds can mitigate the dendrites growth and stabilize the lithium metal anode. However, isolated channels without interconnection hinder the ions transport, which not only aggravates the ion concentration difference inside the channels, but also adversely affect the rate capability of the assembled battery.

Here, TiO_2 frameworks composed of ordered hollow spheres were coated on copper foil as hosts for stabilizing lithium metal anodes. The conductivity difference between TiO_2 and copper makes the lithium prefer to deposit on the copper foil at initial stage, and then gradually fills the TiO_2 framework from bottom to top. Furthermore, hollow spheres in framework were

[a] L. Pan, J. Wang, Z. Luo, Z. Zhao, Y. Li, I. Egun, Prof. H. He
Department of New Energy Technology
Ningbo Institute of Materials Technology and Engineering
Chinese Academy of Sciences
Ningbo 315201, P.R. China
E-mail: hehaiyong@nimte.ac.cn
[b] Z. Luo
University of Chinese Academy of Sciences
Beijing 100049, P.R. China

Supporting information for this article is available on the WWW under https://doi.org/10.1002/batt.202000001

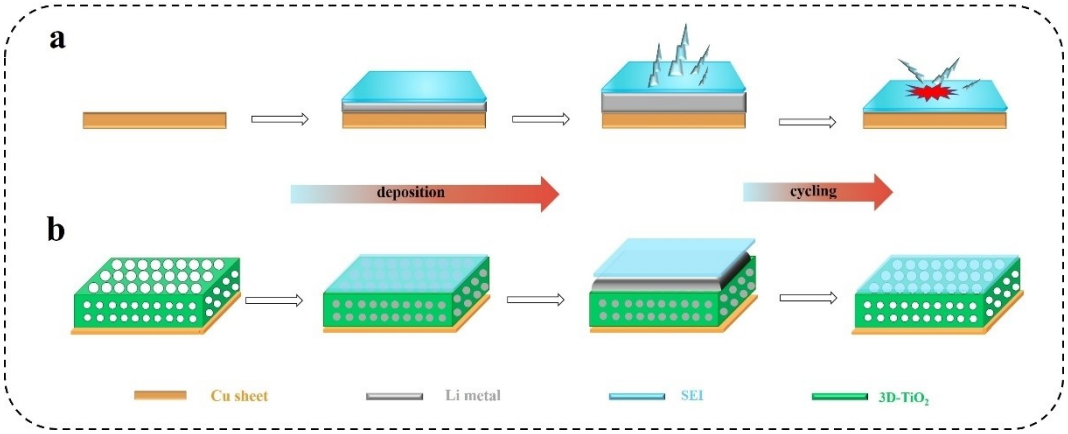

Figure 1. Schematic diagrams of lithium deposition on a) copper foil and b) 3D-TiO_2 electrode

interconnected by holes on the walls to form periodic ion transport channels. These channels shortened ion transport distance and reduced concentration difference between top and inner space of frameworks, preventing the deposition of lithium on surface (Figure 1b). Resultantly, dendrite-free lithium metal anodes were obtained even at high current density and capacity.

2. Results and Discussion

The 3D-TiO_2 electrode was fabricated in three steps: first, self-assembling polystyrene beads on copper foil by vertical deposition method (Figure S1); followed by infiltrating $TiCl_4$ on assembled template by dip-coating; Finally, removal of polystyrene beads through calcination to generate 3D interconnected TiO_2 frameworks (Figure 2a). Through vertical deposition method, polystyrene beads were orderly arrayed in the copper foil to form an opal structure (Figure 2b). The preparation of opal structure provided a guarantee for the subsequent 3D periodic framework. After infiltrating the assembled template with $TiCl_4$ solution, the space between polystyrene beads were occupied by titanium compound due to the hydrolysis of $TiCl_4$ solution (Figure 2c). Eventually, the 3D periodic TiO_2 frameworks were successful prepared by calcination to remove the polystyrene beads template and form TiO_2 at the same time (Figure 2d). Raman spectrum of 3D-TiO_2 electrode shows peaks at 147, 199, 398, 514, 635 cm^{-1} respectively, which belongs to typical anatase TiO_2 Raman characteristic peaks (Figure S2).[25] The X-Ray Diffraction result was consistent with the Raman spectrum, further confirming the successful preparation of TiO_2. The weak intensity of the peaks is due to the relatively low loading of TiO_2 compared to the copper foil (Figure S3).[26] The date of either Raman or XRD characterization confirms the formation of TiO_2 by heat treatment after $TiCl_4$ hydrolysis.

The lithium deposition behavior with various capacity was investigated in coin cells. The initial deposition site of lithium metal, on top of framework or copper foil, is important for

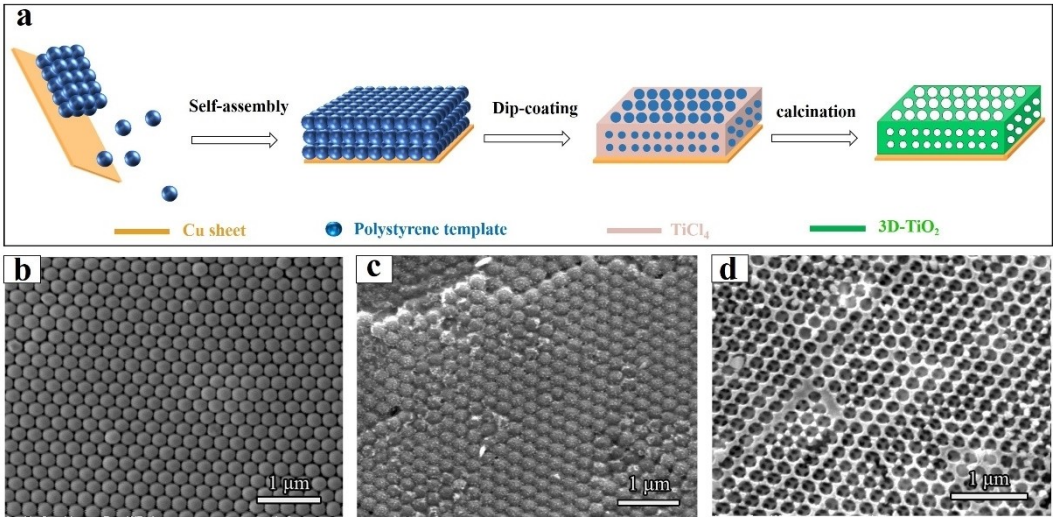

Figure 2. a) Schematic diagram of fabrication of 3D-TiO_2 electrode; b, c, d) SEM image of (b) polystyrene beads template on copper foil, c) polystyrene beads template after dip-coating with $TiCl_4$ and d) 3D-TiO_2 electrode.

subsequent lithium deposition. Thus, surface morphologies were observed by SEM after loading lithium metal. When the area capacity was 1 mA h cm^{-2}, smooth lithium deposition was observed inside the framework (Figure 3a). This result demonstrated that lithium is preferentially deposited into inner space of the framework because of the high conductivity of copper foil. Increasing the area capacity to 3 mA h cm^{-2}, the 3D-TiO_2 framework is full of lithium metal and metallic lithium was also detected on its surface (Figure 3b). Further increase, the capacity of lithium deposition was pushed to 5 mA h cm^{-2}, the surface of 3D-TiO_2 framework was fully covered, but without visible dendritic or mossy lithium (Figure 3c). It was thought that 3D-TiO_2 framework can act as a redistributor to regulate lithium ions, suppressing the fluctuation of lithium ion, and thus prevent the growth of lithium dendrites.[27] In contrast, lithium deposition on copper foil was irregular because of the fluctuation of lithium ions on the surface (Figure 3d). As the loading of the lithium was enhanced to 3 and 5 mA h cm^{-2}, initial uneven deposition accelerates the lithium dendritic growth (Figure 3e and 3f). By analyzing above results, it is rational that the increase in thickness of inverse opal TiO_2 will provide more space for the storage of lithium metal and minimize the volume expansion caused by lithium deposition, improving the storage capacity of electrode. However, TiO_2 is a semiconductor, and thus the increase of thickness will decrease conductivity of electrode. Therefore, in this work, the thickness of TiO_2 layer was not further increased.

This result was consistent with the previous report that the initial nucleation and deposition plays a dominant effect on subsequent deposition behavior.[28] To demonstrate the function of 3D periodic framework, the lithium deposition behavior on TiO_2 surface was investigated. As expected, plenteous dendritic and mossy lithium metal was found on TiO_2 surface, even more than pure copper foil (Figure 3g). It was believed that TiO_2 coating on the copper foil not only increased nucleation free-energy barrier of lithium, but also reduced the conductivity of electrode. Both intensified the growth of mossy and dendritic lithium (Figure 3h and 3i). Effect of cycling on lithium deposition behavior was further investigated to verify the function of 3D framework. After 30 cycles, smooth plating of lithium was observed in 3D-TiO_2 electrode with a loading capacity of 8 mA h cm^{-2}, as a result of abundant 3D ion conduction channels can disperse the concentrated lithium ions to realize a uniform distribution on the electrode. Unfortunately, the situation of lithium deposition on TiO_2 electrode was different, although it possesses the same composition as 3D-TiO_2 electrode, except physical structure. Large amount of mossy lithium appeared on the TiO_2 electrode surface under the same test conditions (Figure S4). The above results showed that the lithium deposition behavior can be

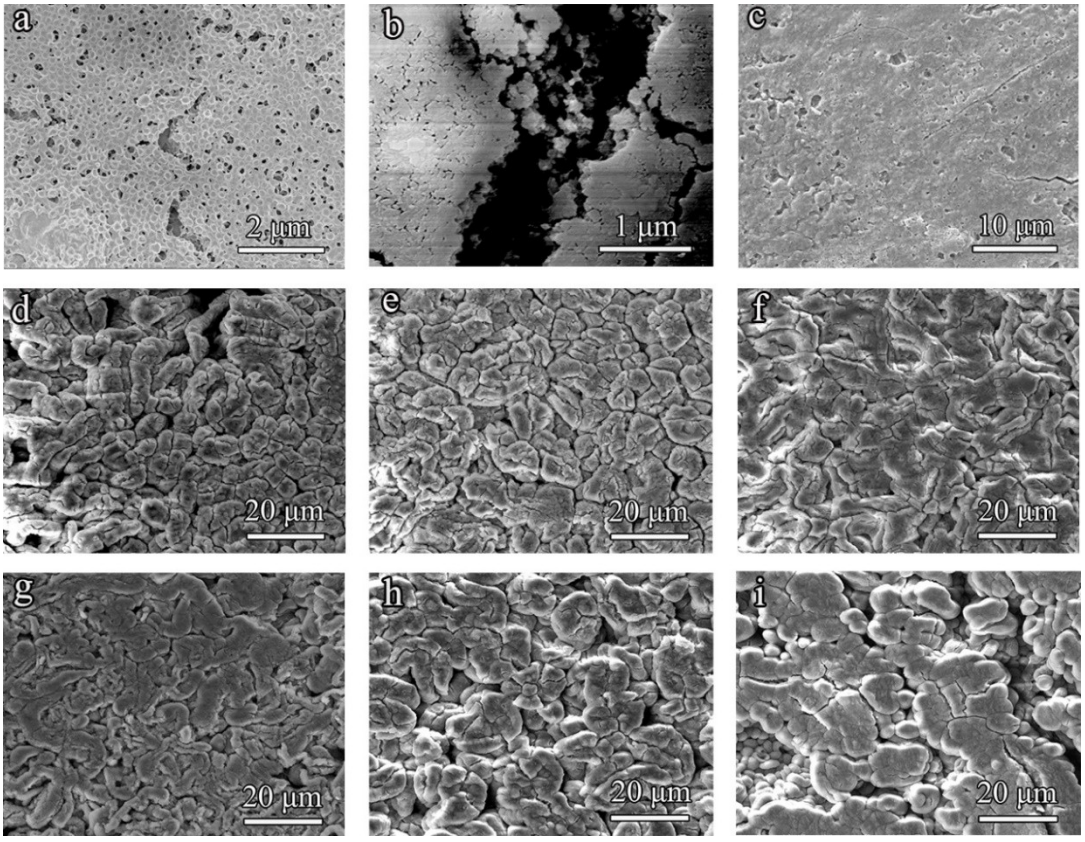

Figure 3. SEM images of 3D-TiO_2 electrodes after a) 1 mA h cm^{-2}, b) 3 mA h cm^{-2} and c) 5 mA h cm^{-2} lithium deposition. SEM images of Cu electrodes after d) 1 mA h cm^{-2}, e) 3 mA h cm^{-2} and f) 5 mA h cm^{-2} lithium deposition. SEM images of TiO_2 electrodes after g) 1 mA h cm^{-2}, h) 3 mA h cm^{-2} and i) 5 mA h cm^{-2} lithium deposition.

regulated by physical structure without the precious metals or dopants.

As an anode, Coulombic efficiency is important for its practical application. Thus, half-cells were assembled using 3D-TiO_2 framework electrode as work electrode and lithium foil as a counter electrode. The Coulombic efficiency was investigated in various current density and area capacity. For area capacity of 1 mA h cm^{-2} and current density of 1 mA cm^{-2}, the 3D-TiO_2 electrode exhibited high and stable average Coulombic efficiency of ~98.0% for 150 cycles. Expectedly, the Cu electrode showed rapid decay to below 80% after 45 cycles (Figure 4a, Figure S5a). When the current density was enhanced to 3 mA cm^{-2}, the average Coulombic efficiency of 3D-TiO_2 electrode was still stable at ~97.2% for 100 cycles. However, Cu electrode revealed a shape decrease to 72.4% after 30 cycles (Figure 4b, Figure S5b). To confirm the role of 3D ion channels within the scaffold in improving the electrochemical performance, the Coulombic efficiency of coin cells assembly by 3D-TiO_2 electrode and TiO_2 electrode were compared (Figure S6). The cells with 3D-TiO_2 electrode displayed a stable Coulombic efficiency for 150 cycles. However, TiO_2 electrode assembly batteries showed a poor cycling stability, even inferior to Cu electrode. This is mainly due to the TiO_2 coated on Cu foil exists in a thin film with solid particles (Figure S7). This electrochemical difference demonstrated that the 3D ion channels contributed to the stability of lithium metal anode. To further confirm the effect of 3D periodic ion channels on electrochemical performance, TiO_2 fiber electrode was also prepared in this study (Figure S8).[29] The electrochemical performance for TiO_2 fiber electrode, was superior to Cu and TiO_2 electrode, but inferior to 3D-TiO_2 electrode (Figure S6). It was thought that the non-periodic channels among the TiO_2 fiber makes it difficult to shorten ion transport distance and optimize the concentration difference between surface and inner space of 3D frameworks.

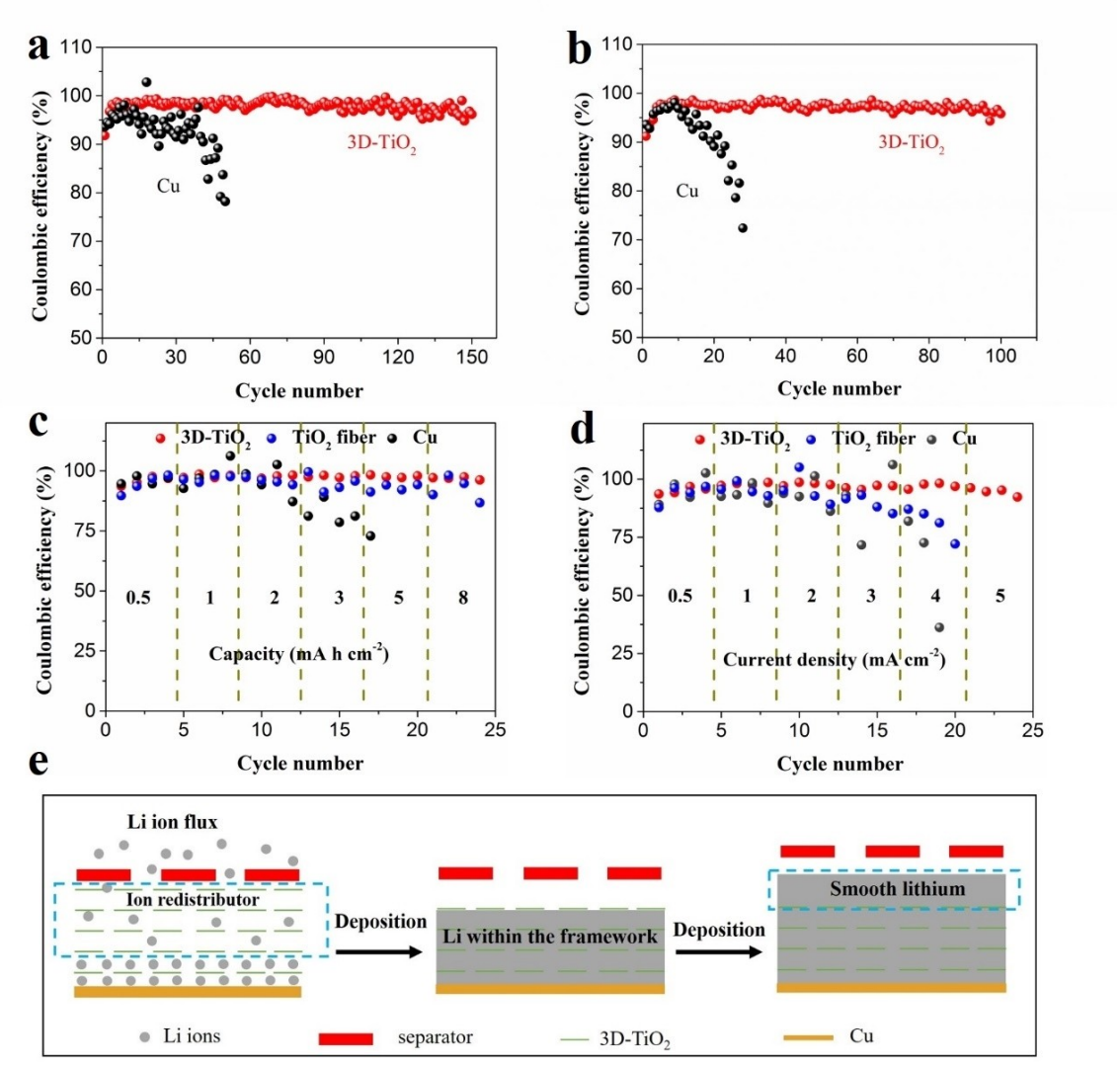

Figure 4. Coulombic efficiency of Cu foil and 3D-TiO_2 at a) 1 mA cm^{-2} and b) 3 mA cm^{-2} for 1 mA h cm^{-2}. c) Cycling stability of lithium plating/stripping on the 3D-TiO_2, Cu and TiO_2 fiber electrode with increased capacity at current density of 1 mA cm^{-2}. d) Cycling stability of lithium plating/stripping on the 3D-TiO_2, Cu and TiO_2 fiber electrode with increased current density for 1 mA h cm^{-2}. (e) Schematic illustration of lithium ions transport and deposition behavior in 3D-TiO_2 electrode.

Additionally, flat plating/stripping voltage plateau showed the mass-transfer overpotential of ~45 mV for first cycle, and gradually reduced to 22 and 16 mV after 30 and 50 cycles respectively (Figure S9). Lower overpotential indicates the fast kinetics of lithium ions migration and superior interface performance realized by the periodic channels in 3D-TiO_2 electrode.

The performance at higher plating/stripping capacity and current density were also tested. A gradual increase in capacity from 0.5 to 8 mA h cm^{-2} showed that the 3D-TiO_2 electrode could maintain a stable Coulombic efficiency of ~97.6% with 8 mA h cm^{-2} lithium deposition. In contrast, Cu electrode abruptly dropped below 75% over 3 mA h cm^{-2}. The high stability of 3D-TiO_2 electrode after mounting plating/stripping capacity was mainly attributed to large space provided by the 3D periodic framework to bear sudden volumetric change. Additionally, uniform lithium deposition minimizing the fracture of SEI films, also benefits the stability of 3D-TiO_2 electrode.[30] Thanks to the random pores among fibers, TiO_2 fiber electrodes also display a relatively stable electrochemical performance in higher lithium deposition capacity compared with Cu foil (Figure 4c). As an important parameter for LIBs, rate capability was also measured as shown in Figure 4d. When the current density was enhanced from 0.5 to 5 mA cm^{-2}, 3D-TiO_2 electrode exhibited average Coulombic efficiency of ~94.6% even at 5 mA cm^{-2}, while TiO_2 fiber electrode dropped below 75% at 4 mA cm^{-2}. This superior rate performance of the 3D-TiO_2 electrode was mainly ascribed to the 3D periodic ion channels facilitating lithium transport. For TiO_2 fiber electrode, pores among fibers are also connected with each other, but without the periodic channels structure, where the ion diffusion distance and resistance are both higher than that of 3D-TiO_2. Thus, as current density is amplified, the Columbic efficiency decrease. Large inner space and 3D periodic ion transport channel make 3D-TiO_2 electrode have high areal capacity and rate capability (Figure 4e).

The cycling stability were tested in symmetric batteries consisting of two identical electrodes. Electrodes were prepared by pre-loading 2 mA h cm^{-2} lithium into the 3D-TiO_2, and then plating/stripping 1 mA h cm^{-2} at various current density. As shown in Figure 5a, the voltage hysteresis of lithium foil electrode gradually increases after 60 h. The hysteresis value of pure lithium foil was four times than that of 3D-TiO_2@Li electrode at 150 cycles. In contrast, the symmetric batteries with 3D-TiO_2 @Li electrode showed smaller voltage hysteresis of ~20 mV and remained unchanged more than 300 h. This result proved that 3D-TiO_2 can effectively stabilize lithium metal anode by improving the lithium ions transport and deposition.[31] The voltage profiles selected from different cycling stages are shown in Figure S10. Both the pure lithium foil and 3D-TiO_2@Li electrode exhibited small voltage hysteresis at 10th cycles due to the formation of stable SEI film. After 50 cycles, the 3D-TiO_2 electrode still demonstrated a small voltage hysteresis. However, the voltage hysteresis of lithium foil

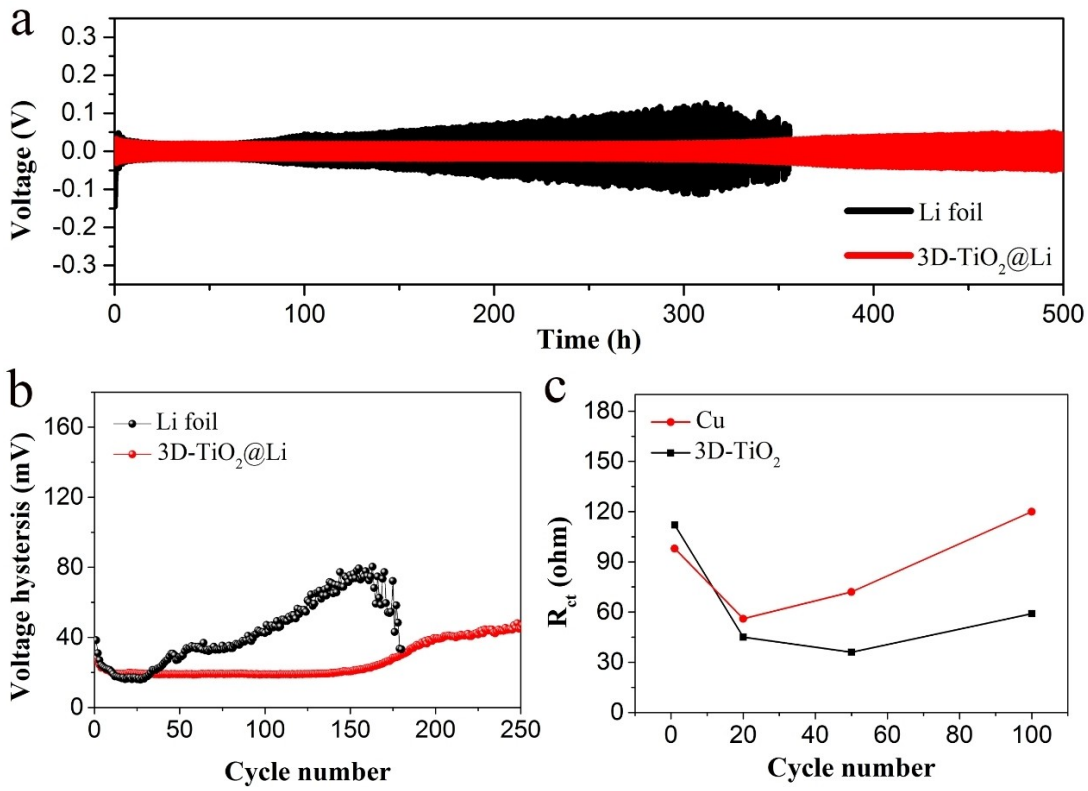

Figure 5. a) Voltage profiles of lithium plating/stripping in lithium foil and 3D-TiO_2@Li symmetric cells with current density of 1 mA cm^{-2} for 1 mA h cm^{-2}. b) Average voltage hysteresis of the lithium plating/stripping process in lithium foil and 3D-TiO_2@Li symmetric cells with current density of 1 mA cm^{-2} for 1 mA h cm^{-2}. c) Variation tendency of impedance of Cu foil and 3D-TiO_2 electrode at different cycles.

electrode was expanded to 30 mV, noise can be found in voltage profile in both 100th and 150th cycles, indicating a negative effect of stability. As the current density is extended to 2 and 4 mA cm^{-2}, similar results were observed. At a current density of 2 mA cm^{-2}, symmetric batteries with lithium foil electrode showed a larger hysteresis loop at initial stage, and gradually increased with cycling. For 3D-TiO_2@Li electrode, the lower average voltage hysteresis of ~60 mV was observed (Figure S11). More aggressively, when the current density enlarged to 4 mA cm^{-2}, 3D-TiO_2@Li symmetric batteries still maintained stable cycling for 125 h, over 250 cycles (Figure S12). It is clear that the voltage hysteresis of pure lithium foil electrode became more serious, as the charge-discharge current density increased. However, the hysteresis of 3D-TiO_2@Li electrode was different (Figure S13). This result was mainly ascribed to the rational structure of the 3D-TiO_2 that provided uniformized charge transfer and lithium ions distribution during cycling thanks to the 3D periodic framework.[32] Additionally, the variation trend of electrochemical impedance was also summarized to evaluate the interfacial transport behaviors of 3D-TiO_2 electrode (Figure 5c). The increased impedance of the Cu electrode after the 20th cycles was mainly attributed to the fracture of SEI film and the formation of "dead" lithium. In comparison, 3D-TiO_2 electrode exhibited a gradual decrease after the initial cycle. The small impedance suggests that stable interface and uniform lithium deposition were achieved within 3D-TiO_2 electrode because of the 3D periodic structure. The lower and stable impedance value of 3D-TiO_2 electrode reflected the excellent interfacial stability, which was also the intrinsic reason for high Coulomb efficiency and low voltage hysteresis.[33]

3. Conclusions

In summary, an inverse opal TiO_2 framework host was fabricated by dip-coating method using polystyrene beads as sacrificial template. The conductivity difference between copper foil and TiO_2 prefers metallic lithium to nucleate on copper foil, and then stuff the framework from bottom of framework. This novel design avoids the metallic lithium to deposit on top of framework before the cram of inner space. In addition, 3D periodic channels in electrode reduces the ions concentration fluctuation to realize the uniform lithium deposition. Consequently, 3D-TiO_2 electrode showed a high Coulombic efficiency even at high capacity. Additionally, fast ion transport channel built by 3D periodic framework improved the rate capability of electrode, owning to the shortened ion transport distance. We believed that the 3D-TiO_2 electrode design will provide a novel strategy for obtaining high-energy density and high-power density lithium metal anodes.

Experimental Section

Synthesis of materials

Synthesis of polystyrene (PS) beads

Styrene was first purified by vacuum distillation to remove the stabilizer. 20 mL purified styrene, 0.75 g PVP, and 150 mL deionized water were added into a 250 mL triple-neck. After bubbling with N_2 for 20 min, the mixture was then fluxed at 60 °C under magnetic stirring for 30 min. Subsequently, 15 mL aqueous solution containing 0.3 g $K_2S_2O_8$ was added into the flask to initiate the polymerization reaction. After stirring for 24 h, the synthesized polystyrene beads were centrifuged and washed several times. Finally, the synthesized polystyrene beads were dissolved in water to prepare a solution and placed in the refrigerator for further using.

Self-assembly of PS beads on copper foil

The Cu foil was firstly cleaned to remove surface organic composition and oxides, and dry at N_2 atmosphere. Then, Cu foils were set tilted at a 60° with each sample placed individually in small bottles, and 2 mL PS solution was carefully dispensed into the bottles. Finally, the bottles were placed into the oven and set to the desired temperature of 70 °C till the completion of deposition. After the deposition, Cu foil with PS beads were annealed on an oven at 90 °C for 6 h to remove remaining solvent and ensure good contact of the template beads with the substrate.

Synthesis of 3D-TiO_2 framework

The preparation of 3D-TiO_2 framework was as follows: First, 1 mL $TiCl_4$ was added into 50 mL anhydrous ethanol to prepare $TiCl_4$ solution. Second, 20 uL prepared $TiCl_4$ solution was directly dip-coating on Cu foils assembled with PS beads template, and dried at room temperature. Finally, the 3D-TiO_2 framework was obtained by thermal annealing in a tube furnace at 450 °C at argon atmosphere for 3 h (2 °C min^{-1}). The TiO_2 electrodes used for comparison in this work were fabricated through directly dip-coating on Cu foil with $TiCl_4$ solution and thermal annealing.

Electrochemical tests

Coulomb efficiency and cycling stability of Li plating/stripping were performed by assembling 3D-TiO_2/Li half cells in glovebox and testing by a battery testing system (LandCT2001 from LAND electronics Co, Ltd). 3D-TiO_2, TiO_2, and Cu were used as work electrodes, Li foils were used as reference electrodes. Celgard separators (18 mm in diameter and 20 μm in thickness) were adopted to separate the positive and negative electrodes. 1 M LiTFSI dissolved in 1:1 DOL/DME with 1% w/w $LiNO_3$ (70 μL) was used as electrolyte.

The mechanism of lithium insertion and delithiation of titanium dioxide is as follow: $TiO_2 + xLi^+ + xe^- \leftrightarrow LixTiO_2$ (lithium insertion potential: 1.6 ~ 1.8 V). During the first cycle of discharge process of half-cell assembly by 3D-TiO_2 electrode, Li_xTiO_2 was formed after intercalation of lithium ions, which consumes a certain amount of lithium ions. Therefore, pre-cycling was adopted in this study to improve the initial Coulombic efficiency and form a stable SEI film.

Polarization performance and cycling stability of Li plating/stripping were performed by assembling 3D-TiO_2@Li and Li foil symmetric batteries respectively. The 3D-TiO_2@Li electrodes were taken out from pre-processed half cells, and washed multiple times

with DOL or DME to remove the residual electrolyte and salt. Two 3D-TiO_2@Li electrodes were reassembled into symmetric batteries with electrolyte (1 M LiTFSI dissolved in 1:1 DOL/DME with 1% w/w $LiNO_3$,70 μL). The Li symmetric batteries were assembled with two Li foil (16 mm) and same electrolyte.

The ionic interfacial transport behavior was studied using electrochemical impedance spectroscopy (EIS) spectra in the frequency range from 1×10^{-1} to 1×10^{5} Hz with a voltage perturbation of 5 mV.

Electrodes characterization

After the cycling, the electrodes were disassembled in glovebox, and then washed multiple times with DOL or DME to remove the residual electrolyte and salt. The surface morphology analysis was performed using scanning electron microscopy (SEM, FEI, Sirion200). The X-ray diffraction (XRD) were adopted to characterize the crystalline phase with an X-ray diffractometer (Bruker D8 advanced diffractometer) using Cu Ka ($\lambda = 1.5406$ Å) radiation. Raman spectra were acquired with a Renishaw in Via reflex Raman spectrometer at an excitation wavelength of 532 nm from an Nd: YAG (neodymium-doped yttrium aluminum garnet) laser operating at 120 mW.

Acknowledgements

This work was supported by the Hundred Talents program, the National Natural Science Foundation of China (Grant No. 51872304) and Ningbo S&T Innovation 2025 Major Special Program (2018B10024).

Conflict of Interest

The authors declare no conflict of interest.

Keywords: 3D periodic structure · ion transport channel · lithium dendrite · lithium metal anode · batteries

[1] J.-M. Tarascon, M. Armand, *Materials* for *Sustainable Energy*, 171–179.
[2] Y. X. Yin, S. Xin, Y. G. Guo, L. J. Wan, *Angew. Chem. Int. Ed. Engl.* **2013**, *52*, 13186–13200.
[3] M. Li, J. Lu, Z. Chen, K. Amine, *Adv. Mater.* **2018**, e1800561.
[4] J. B. Goodenough, Y. Kim, *Chem. Mater.* **2010**, *22*, 587–603.
[5] W. Xu, J. Wang, F. Ding, X. Chen, E. Nasybulin, Y. Zhang, J.-G. Zhang, *Energy Environ. Sci.* **2014**, *7*, 513–537.
[6] D. Aurbach, E. Zinigrad, H. Teller, Y. Cohen, G. Salitra, H. Yamin, P. Dan, E. Elster, **2002**, *149*, A1267-A1277.
[7] S. Chandrashekar, N. M. Trease, H. J. Chang, L. S. Du, C. P. Grey, A. Jerschow, *Nat. Mater.* **2012**, *11*, 311–315.
[8] L. Li, S. Li, Y. Lu, *Chem. Commun. (Camb.)* **2018**, *54*, 6648–6661.
[9] Q. Pang, X. Liang, A. Shyamsunder, L. F. Nazar, *Joule* **2017**, *1*, 871–886.
[10] Z. Huang, J. Ren, W. Zhang, M. Xie, Y. Li, D. Sun, Y. Shen, Y. Huang, *Adv. Mater.* **2018**, *30*, e1803270.
[11] Q. Wang, C. Yang, J. Yang, K. Wu, C. Hu, J. Lu, W. Liu, X. Sun, J. Iu, H. Zhou, *Adv. Mater.* **2019**, *31*, e1903248.
[12] N. W. Li, Y. X. Yin, C. P. Yang, Y. G. Guo, *Adv. Mater.* **2016**, *28*, 1853–1858.
[13] M. Wang, Z. Peng, W. Luo, F. Ren, Z. Li, Q. Zhang, H. He, C. Ouyang, D. Wang, *Adv. Energy Mater.* **2019**, *9*.
[14] J. Dai, C. Yang, C. Wang, G. Pastel, L. Hu, *Adv. Mater.* **2018**, *30*, e1802068.
[15] R. Chen, Q. Li, X. Yu, L. Chen, H. Li, *Chem. Rev.* 2019.
[16] S. Xia, X. Wu, Z. Zhang, Y. Cui, W. Liu, *Chem* **2019**, *5*, 753–785.
[17] G. Zheng, S. W. Lee, Z. Liang, H. W. Lee, K. Yan, H. Yao, H. Wang, W. Li, S. Chu, Y. Cui, *Nat. Nanotechnol.* **2014**, *9*, 618–623.
[18] L. L. Lu, J. Ge, J. N. Yang, S. M. Chen, H. B. Yao, F. Zhou, S. H. Yu, *Nano Lett.* **2016**, *16*, 4431–4437.
[19] T. T. Zuo, X. W. Wu, C. P. Yang, Y. X. Yin, H. Ye, N. W. Li, Y. G. Guo, *Adv. Mater.* **2017**, *29*.
[20] K.-H. Chen, A. J. Sanchez, E. Kazyak, A. L. Davis, N. P. Dasgupta, *Adv. Energy Mater.* **2019**, *9*.
[21] L. Liu, Y. X. Yin, J. Y. Li, S. H. Wang, Y. G. Guo, L. J. Wan, *Adv. Mater.* **2018**, *30*.
[22] J. Pu, J. Li, Z. Shen, C. Zhong, J. Liu, H. Ma, J. Zhu, H. Zhang, P. V. Braun, *Adv. Funct. Mater.* **2018**, *28*.
[23] K. Tantratian, D. X. Cao, A. Abdelaziz, X. Sun, J. Z. Sheng, A. Natan, L. Chen, H. L. Zhu, *Adv. Energy Mater.* **2019**, *1902819*.
[24] S. H. Wang, Y. X. Yin, T. T. Zuo, W. Dong, J. Y. Li, J. L. Shi, C. H. Zhang, N. W. Li, C. J. Li, Y. G. Guo, *Adv. Mater.* **2017**, *29*.
[25] Y.-H. Zhang, C. K. Chan, J. F. Porter, W. Guo, *J. Mater. Res.* **1998**, *13*, 2602–2609.
[26] G. Lui, G. Li, X. Wang, G. Jiang, E. Lin, M. Fowler, A. Yu, Z. Chen, *Nano Energy* **2016**, *24*, 72–77.
[27] C.-Z. Zhao, P.-Y. Chen, R. Zhang, X. Chen, B.-Q. Li, X.-Q. Zhang, X.-B. Cheng, Q. Zhang, 2018, 4, eaat3446.
[28] T. Wang, P. Zhai, D. Legut, L. Wang, X. Liu, B. Li, C. Dong, Y. Fan, Y. Gong, Q. Zhang, *Adv. Energy Mater.* **2019**, *9*.
[29] C.-M. Tsai, C.-G. Song, Y.-C. Hung, Y.-G. Jeong, S. H. Oh, J. H. Jeong, H. Kim, H. Huh, J.-W. Yoon, W. Sigmund, *Ceram. Int.* **2017**, *43*, 3761–3768.
[30] Y. Zhao, X. Yang, Q. Sun, X. Gao, X. Lin, C. Wang, F. Zhao, Y. Sun, K. R. Adair, R. Li, M. Cai, X. Sun, *Energy Storage Mater.* **2018**, *15*, 415–421.
[31] A. M. Hafez, Y. Jiao, J. Shi, Y. Ma, D. Cao, Y. Liu, H. Zhu, *Adv. Mater.* **2018**, *30*, e1802156.
[32] F. Ren, Z. Peng, M. Wang, Y. Xie, Z. Li, H. Wan, H. Lin, D. Wang, *Energy Storage Mater.* **2019**, *16*, 364–373.
[33] J. Qian, W. A. Henderson, W. Xu, P. Bhattacharya, M. Engelhard, O. Borodin, J. G. Zhang, *Nat. Commun.* **2015**, *6*, 6362.

Manuscript received: January 2, 2020
Revised manuscript received: March 8, 2020
Accepted manuscript online: March 15, 2020
Version of record online: April 3, 2020